

Attribution of Urban Diurnal Thermal Environmental Change: Importance of Global–Local Effects

Wenbo Yu , Jun Yang , Nan Cong , Jiayi Ren , Huisheng Yu , Xiangming Xiao , and Jianhong Xia 

Abstract—Global climate change is causing various negative impacts on urban ecosystems and energy systems. To effectively mitigate and adapt to these changes, it is important to understand the contributions of background climate and local effects to urban thermal environment variation. This study utilized the empirical orthogonal function (EOF) approach to deconstruct long-term MODIS land surface temperature (LST) datasets to obtain the main features of change in daytime and nighttime thermal environments. Local bivariate spatial autocorrelation analysis was used to explore the underlying causes of these changes. The main EOF modes explained 73.14% and 81.33% of daytime and nighttime thermal environment variation, respectively. The correlation coefficient between the time coefficient of the main modes and the average LST was > 0.99 , reflecting the role of global effect caused by background climate change. The secondary EOF modes explained 12.51% and 4.12% of daytime and nighttime thermal environment variation, respectively, and were spatially correlated with changes in landscape thermal intensity, reflecting local effect caused by landscape change and anthropogenic heat emissions. In expansion and renewal areas, industrial zones and compact high-rise buildings had the most obvious warming effect on the daytime thermal environment, while mid-to-high-rise buildings had the most obvious warming effect on the nighttime thermal environment. The results of this study provide valuable insights into the mechanisms of background climate and local effects on the urban thermal environment, and provide a reference for formulating effective strategies for mitigating and adapting to change in urban areas, and for promoting sustainable development.

Index Terms—Changes in thermal environment, empirical orthogonal functions, local climate zone, mitigation and adaptation strategies, Shenyang city.

Manuscript received 3 July 2023; revised 6 August 2023; accepted 19 August 2023. Date of publication 23 August 2023; date of current version 12 September 2023. This work was supported in part by the National Natural Science Foundation of China under Grant 41771178, Grant 42030409, and Grant 41671151, and in part by the Fundamental Research Funds for the Central Universities under Grant N2111003. (Corresponding authors: Jun Yang; Nan Cong.)

Wenbo Yu, Jiayi Ren, and Huisheng Yu are with the Northeastern University, Shenyang 110169, China (e-mail: 2110013@stu.neu.edu.cn; 2210011@stu.neu.edu.cn; 1810019@stu.neu.edu.cn).

Jun Yang is with the Human Settlements Research Center, Liaoning Normal University, Dalian 116029, China, and also with the Jangho Architecture College, Northeastern University, Shenyang 110169, China (e-mail: yangjun8@mail.neu.edu.cn).

Nan Cong is with the Key Laboratory of Ecosystem Network Observation and Modeling, Institute of Geographic Sciences and Natural Resources Research, Chinese Academy of Sciences, Beijing 100101, China (e-mail: congnan@igsnrr.ac.cn).

Xiangming Xiao is with the Department of Microbiology and Plant Biology, Center for Spatial Analysis, University of Oklahoma, Norman, CO 73019 USA (e-mail: xiangming.xiao@ou.edu).

Jianhong Xia is with the School of Earth and Planetary Sciences, Curtin University, Perth 65630, Australia (e-mail: c.xia@curtin.edu.au).

Digital Object Identifier 10.1109/JSTARS.2023.3308045

I. INTRODUCTION

GLOBAL climate change is the greatest challenge facing humanity in the 21st century. Intensified thermal environmental changes are the most direct result of climate change. The Intergovernmental Panel on Climate Change noted that global climate change would cause most human settlements to suffer from extreme heat and that climate-related health risks are expected to increase [1], [2]. In urban areas, this can exacerbate health problems such as heat stroke, dehydration, and cardiovascular disease, and has widespread negative impacts on urban ecosystems and energy systems [3]. The United Nations' (UN) Sustainable Development Goal 13, "Taking urgent action to combat climate change and its impacts," requires that climate change responses be integrated into national strategies, and plans [4], and that clear attribution of thermal environmental change is a prerequisite for climate change measures.

The classical Lowry framework decomposes the measured values of meteorological elements into a linear sum of background climate, local landscape, and local urbanization effects [5]. The background climate effect reflects the overall temperature, humidity, wind speed, atmospheric turbidity, and other atmospheric transport conditions, and its changes are mainly triggered by excessive greenhouse gas emissions [6], [7]. Local landscape effects reflect the emissivity, albedo, and topographic relief of the urban subsurface. These changes are mainly caused by changes in subsurface properties due to rapid urban expansion and renewal [8], [9]. The resulting urban heat island effect, in which urban temperatures are higher than those in the suburbs, is also the most significant feature of the changing urban thermal environment [10], [11]. Currently, the rate of increase in land surface temperature (LST) in urban regions is 29% higher than that in rural regions, exposing urban residents to more severe thermal hazards [12]. To determine the contribution of urban development to local landscape effects, scholars have analyzed the influence of 2-D subsurface features and 3-D building features of the landscape on the thermal environment [13], [14], [15]. Typically, vegetation and impermeable surfaces have the most significant effects on the LST. When impervious surface coverage is $> 60\%$, there is a significant warming effect [16]. Landscape diversity also has a notable effect on the spatial heterogeneity of the urban thermal environment [17]. The local urbanization effect is a specific manifestation of climate change within cities and consists mainly of thermal emissions from human activities. This has a strong impact on urban canopy heat island and a weaker impact on surface heat island [18].

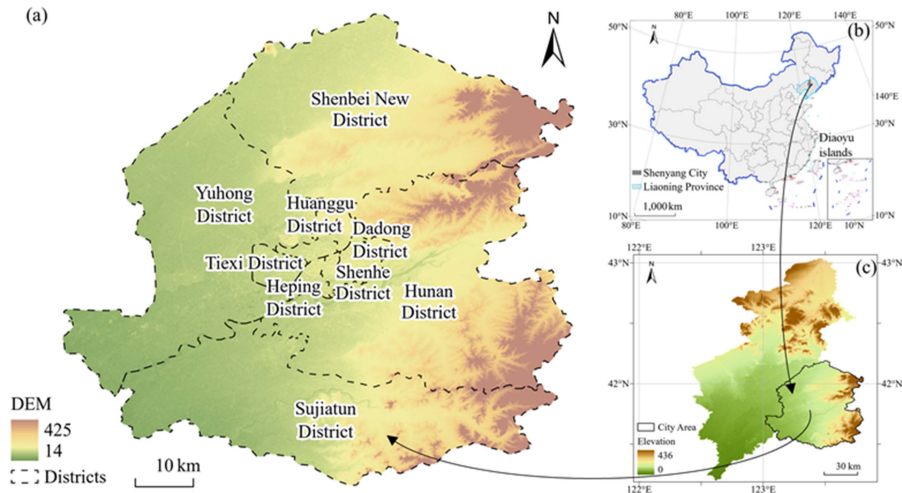


Fig. 1. Overview of the study area. (a) Administrative division of Shenyang city district. (b) Location of Shenyang city in China. (c) Location of Shenyang City district.

As can be seen from the above, most studies have focused on analyzing the impact of a single effect on the thermal environment; in contrast, the contribution rates and interaction relationships of multiple effects on changes in the thermal environment remain unclear. The empirical orthogonal function (EOF) is an effective method for decomposing spatiotemporal observational data into a set of mutually orthogonal spatial patterns and their corresponding temporal patterns. Currently, this method is widely used for temperature and circulation feature extraction in oceans [19], [20], wind field simulation [21], [22], precipitation [23], and other macroscale climatological analyses. The aim of this study was to apply the EOF method to obtain stable characteristics of daytime and nighttime thermal environment variation. Unlike previous studies using fixed meteorological station data [24], this article chooses remote sensing Earth observation data as the data source. At present, MODIS and Landsat remote sensing images are widely used in global long-term LST research [25], [26]. Compared to Landsat, MODIS LST data have a low spatial resolution (1 km) but a high temporal resolution (daily), which is beneficial for reducing the interference of abnormal phenomena in long-term thermal environment research [27], [28], [29]. This study obtained the characteristics of thermal environment changes by deconstructing the MODIS LST dataset.

This study determined the influence of global–local effects on thermal environmental change. The global effect, i.e., the influence of the background climate change. Since the effect of background climate on LST is convergent, the global effect can be reflected by the overall mean value of LST in the study area. The local effect, i.e., local landscape and urbanization effects, can be reflected by changes in the properties of the subsurface and anthropogenic thermal emissions. In this study, the local climate zone (LCZ, the definition and actual scenario of LCZ are shown in Appendix Table III) concept proposed by Stewart and Oke [30] was used to reflect local effect. The LCZ classifies urban landscapes according to material, ground cover, structure, and energy metabolism, which allows for significant

TABLE I
MEAN AND STANDARD DEVIATION OF EOF FOR DIFFERENT LCZ IN THE DAYTIME THERMAL ENVIRONMENT

LCZ type	EOF1		EOF2 gt 0		EOF 3	
	Mean	Std.	Mean	Std.	Mean	Std.
LCZ 1	13.18	3.34	15.89	11.00	-5.18	13.76
LCZ 2	11.61	3.38	12.21	10.81	-8.82	12.15
LCZ 3	14.05	2.61	12.27	8.34	-3.06	11.72
LCZ 4	12.46	2.94	12.21	9.22	-4.74	13.50
LCZ 5	10.95	2.79	14.36	9.14	-10.12	11.64
LCZ 6	14.57	2.87	11.44	9.28	-0.48	14.05
LCZ 8	15.16	3.33	19.56	13.52	1.01	13.07
LCZ 9	14.21	2.87	11.24	7.06	-2.41	12.37
LCZ 10	14.11	3.62	17.57	15.37	-2.57	12.67
LCZ A	13.75	2.51	8.29	8.55	1.63	10.09
LCZ B	13.85	2.88	11.27	8.66	-3.63	10.19
LCZ C	14.60	2.65	11.75	8.72	1.56	13.23
LCZ D	13.99	3.55	10.45	9.02	-1.69	15.18
LCZ E	14.10	2.97	15.22	12.01	-4.23	12.85
LCZ G	11.49	3.96	9.28	8.16	-9.42	13.66

differences between landscapes in terms of architectural features and anthropogenic heat emissions [31], [32], [33] and thus local effects of urban growth and renewal can be effectively identified [34], [35]. We also chose to apply earth observation data to classify LCZ through random forests method, which can effectively compensate for the lack of early building vector data.

The novelty of this study lies in the application of Earth observation data over a long period of time to realize the attribution of changes in the urban thermal environment. The results of this study help to further offer a reference to guide the development of future urban mitigation and adaptation strategies for sustainable development.

TABLE II
PERCENTAGE OF LCZ IN THE OUTLIER TYPE AND ITS INFLUENCE ON
THERMAL ENVIRONMENT VARIATION

LCZ type	Outlier percentage			EOF1		EOF2	
	Outliers	Total	Perc.	Mean	Std.	Mean	Std.
LCZ 1	1566	4302	36.40	19.73	2.49	-28.42	13.47
LCZ 2	7468	27284	27.37	19.12	2.93	-26.32	15.43
LCZ 3	1467	10431	14.06	17.37	3.22	-19.19	12.88
LCZ 4	1924	5863	32.82	20.35	4.03	-28.69	16.13
LCZ 5	515	1860	27.69	18.55	3.06	-21.56	11.56
LCZ 6	1916	26443	7.25	17.72	2.88	-17.57	14.12
LCZ 8	8498	33304	25.52	17.15	2.72	-16.97	11.62
LCZ 9	431	2769	15.57	18.29	1.82	-19.08	3.87
LCZ 10	2315	8995	25.74	18.18	3.17	-23.76	15.19
LCZ A	556	28499	1.95	19.44	3.27	-22.71	16.50
LCZ B	1121	9216	12.16	18.53	3.23	-19.02	12.92
LCZ C	864	10198	8.47	19.67	3.67	-20.28	13.24
LCZ D	6318	170075	3.71	17.26	2.64	-15.83	12.41
LCZ E	688	2191	31.40	18.60	2.60	-16.98	13.05
LCZ G	378	6216	6.08	19.71	3.59	-28.37	17.91

II. STUDY AREA AND DATA SOURCES

A. Study Area

Shenyang is located in the northeastern part of China (see Fig. 1), with a predominantly plain topography, and is an important heavy industrial base and grain producing area. Influenced by the monsoon, Shenyang's precipitation is concentrated in the summer, with a large temperature difference and four distinct seasons. The study area includes five central districts (Dandong District, Huanggu District, Shenhe District, Tiexi District, and Heping District) and four suburban districts (Yuhong District, Shenbei New District, Hunnan District, and Sujiatun District) of Shenyang. These districts together constitute the municipal jurisdiction of Shenyang. In 2020, the study area had a population density of 2256 persons/km². Rapid urban growth and high population densities have caused dramatic changes in the thermal environment of the study area. It is essential to clarify the factors driving the changes in the thermal environment.

B. Data

The thermal environment data for this study were derived from the MODIS LST dataset (MOD11A1). The Google Earth Engine platform was used to generate an annual summer (June to August) average LST dataset for the study area from 2001 to 2022, including daytime and nighttime data, with a total of 44 images. Climate zones were classified based on Landsat imagery. Considering the lag in climate impact, the acquisition time points were 2000 and 2020. In addition, images provided by Google Earth were used to create training areas and evaluate accuracy for LCZ classification. The specific data sources are listed in Appendix Table IV.

III. METHODOLOGY

In this study, we decomposed the mean surface temperature dataset using EOF to obtain the time and space modes reflecting thermal environment changes, and explored the influence of global-local effects on changes in the thermal environment. The correlation between the trend of time modes and annual mean LST of the study area was analyzed to determine the association between thermal environment changes and background climate. The correlation between spatial modes and changes in urban form reflected in the LCZ. We plotted the LCZ of the study area for 2000 and 2020 using the LCZ classification method provided by WUDAPT. Since LCZ is a categorical rather than a quantitative concept, it is difficult to directly establish a link between LCZ changes and changes in the thermal environment. Therefore, our idea is to first use a variable to reflect the ability of the urban form represented by LCZ to influence the thermal environment change, then use bivariate spatial autocorrelation to extract the strong correlation region between the variable and the thermal environment change, and finally, to analyze the compositional change and the intensity of the influence of LCZ in the strong correlation region. Through this process, we finally establish a correlation between the LCZ and LST to clarify the local effect. Fig. 2 illustrates the research framework of this study.

A. EOF

EOF is a method for analyzing the structural features of matrix data and extracting the main information. Its main principle decomposes the time series of the field into spatial features that do not vary with time and temporal coefficients that vary with time, and then extracts the main information concentrated in several modal components by eliminating redundant information through the variance contribution rate. The variable values of any space point i and any time point j can be considered as a linear combination of p spatial functions eof_{ik} and time functions PC_{kj} ($k = 1, \dots, p$). Let LST_{set} be the set of LST data, and LST_{set} can be represented as

$$LST_{set} = \begin{bmatrix} LST_{11} & \dots & LST_{1p} \\ \dots & \dots & \dots \\ LST_{n1} & \dots & LST_{np} \end{bmatrix}. \quad (1)$$

Each row represents a time series and each column represents the spatial points of the LST, with n points and p time periods.

The covariance matrix of the time series is derived as

$$C = \frac{1}{p} LST_{set} LST_{set}^T \quad (2)$$

where C represents the covariance matrix, which is the cross product of LST_{set} and its transpose matrix.

For its orthogonal decomposition, we obtain (3)

$$C = E \Lambda E^T = (e_1, e_2, \dots, e_n) \begin{pmatrix} \lambda_1 & \dots & 0 \\ \vdots & \ddots & \vdots \\ 0 & \dots & \lambda_n \end{pmatrix} \begin{pmatrix} e_1^T \\ e_2^T \\ \vdots \\ e_n^T \end{pmatrix} \quad (3)$$

where C represents the covariance matrix, e_i and E represent the i th eigenvector and the composition matrix consisting of

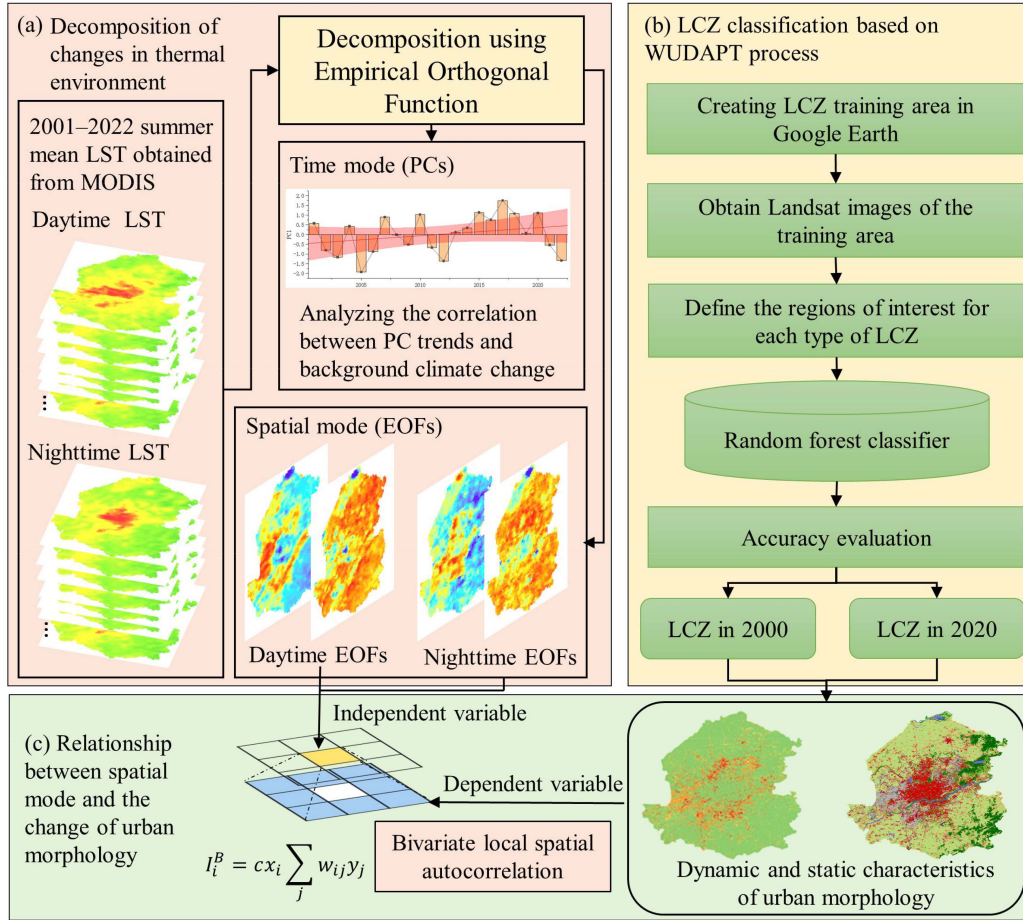


Fig. 2. Research framework. (a) Decomposition of changes in thermal environment. (b) LCZ classification based on the WUDAPT process. (c) Relationship between spatial mode and changes in urban morphology.

the eigenvectors, respectively. Λ and λ_i represent the matrix consisting of eigenvalues and i th eigenvalue, respectively.

The orthogonal decomposition of the spatial domain can be obtained by ranking the eigenvalues according to their values (i.e., $\lambda_1 > \lambda_2 > \dots > \lambda_n$), and then calculating the eigenvectors of $LST_{set} LST_{set}'$. At this point, each nonzero eigenvalue represents the corresponding spatial eigenvector, called the EOF. Projecting the spatial eigenvector onto the original data, we obtained the time coefficient PC:

$$PC = E' LST_{set} \quad (4)$$

where PC represents the time coefficient, which is obtained by multiplying the inverse of the eigenvector matrix E' with the original data matrix.

LST_{set} can be reduced as follows:

$$LST_{set} = EOF \cdot PC + \text{Mean} \quad (5)$$

where EOF and PC represent the spatial modal matrix and its corresponding temporal modal matrix, respectively. Mean represents the mean LST for the study period.

The variance contribution vc_i of each EOF mode was expressed as

$$vc_i = \lambda_i / \left(\sum_{k=1}^p \lambda_k \right) \quad (i = 1, 2, \dots, p). \quad (6)$$

For the randomness of the spatial modes, the North criterion was used to test the error of the feature roots at a 95% confidence level.

B. Changes in Landscape Thermal Intensity (LTI) Based on LCZ

Using the WUDAPT process and referring to the working model developed by Bechtel et al. [36], LCZ mapping was broadly divided into four steps:

Landsat satellite map data preparation;
digitization of the training area on Google Earth;
classification using a random forest classifier in SAGA GIS; and
validation and redefinition of the training area.

In order to quantify the correlation between changes in urban form and the thermal environment, we chose three indicators of building landscape characteristics that have the greatest correlation with the intensity of the thermal environment, namely,

percentage of impervious surface (PIS), building density (BD), and building height (BH), as having the greatest correlation with the intensity of the thermal environment [13]. Then, we developed the LTI variable as a linear function of PIS , BD , and BH . PIS , BD , and BH were estimated based on the average range of the LCZ definitions for each category (see Appendix Table III for detailed range), thus identifying the link between the thermal environmental characteristics of the urban form and the LCZ [30]

$$LTI = k_{PIS}PIS + k_{BD}BD + k_{BH}BH. \quad (7)$$

In this study, k_{PIS} , k_{BD} , and k_{BH} were determined based on the correlations between PIS , BD , BH , and LST. According to Guo et al. [13], this value varies with the urban–rural gradient, and the values of k_{PCL} , k_{BD} , and k_{BH} were taken as 58.44%, 21.41%, and 20.15%, respectively. The degree of variation LTI_{diff} for each spatial location in the study area was expressed as

$$LTI_{diff} = LTI_{2020} - LTI_{2000} \quad (8)$$

where LTI_{2020} and LTI_{2000} represents the LTI for 2020 and 2000, respectively.

According to the changes in the LCZ types, they can be divided into four categories: urban expansion zone (natural type converted to built type), urban renewal zone (built type internally transformed or converted to natural type), urban stability zone (built type unchanged), and natural zone (natural type unchanged or converted to other natural types).

C. Bivariate Local Spatial Autocorrelation Analysis

Spatial correlation characteristics can be explored using the bivariate local spatial autocorrelation (Moran's I) index, and the results indicate the overall spatial correlation between two variables. The local correlation between the independent variable x_i of region i and the dependent variable y_j in region j can be classified into four types: high–high cluster, low–low cluster, high–low outlier, and low–high outlier. The local Moran's I index for region i I_i can be expressed as

$$I_i = cx_i \sum_j w_{ij}y_j \quad (9)$$

where w_{ij} is an element of the spatial weight matrix. In this study, the weight of region j adjacent to the edge or corner of region i was set to 1, and the rest was set to 0.

IV. RESULTS

A. Changes in Urban LCZ

The urban morphological transformation of the study area was analyzed based on changes in the LCZ, as shown in Fig. 3. Fig. 3(a) shows the spatial distribution and percentage change of the LCZ between 2000 and 2020 (see Appendix Table V for mapping accuracy). The percentage of built-up LCZ increased from 23.25% in 2000 to 34.87% in 2020. Among these, the proportion of built-up LCZ increased from 23.25% in 2000 to 34.87% in 2020. Among these, the proportion of LCZ D low vegetation decreased by 16.78%, which was the largest transfer-out category. The proportion of LCZ 8 large low-rise buildings increased by 9.03%, which was the largest transfer in this category. In the built-up LCZ, the

proportion of low-rise buildings showed a decreasing trend, whereas that of high-rise buildings showed an increasing trend. Except for LCZ D and LCZ F, the natural-type LCZs showed an increasing trend, with LCZ C shrubs showing the largest increase of 2.87%. Fig. 3(b) shows the changes in LTI. Fig. 3(b-1) shows the original calculation results at 100 m resolution; to better match the LST, Fig. 3(b-2) resamples the LTI in the range of 1000 m with the mean value. Areas with increased LTI show a circular distribution, mainly located in the four suburbs near the urban center (Hunnan District, Yuhong District, Sujiatun District, and Shenbei New District), which is related to continuous urban expansion behavior. Areas with reduced LTI were mainly located in rural areas southeast of the city. Fig. 3(c) shows the types of urban LCZ changes in which urban stability areas, urban renewal areas, urban expansion areas, and natural areas were distributed hierarchically from the urban center outward, with percentages of 2.47%, 10.82%, 14.99%, and 71.72%, respectively.

B. Influencing Factors of Daytime Thermal Environment Variation

In the deconstruction of the daytime thermal environment using EOF analysis, the first three modes passed the North test and explained 88.81% of the variation in the daytime thermal environment in the study area. The temporal and spatial patterns are shown in Fig. 4, and the mean values of the LCZ in each EOF mode are listed in Table I.

The EOF analysis showed that the variance contribution of the first mode was 73.14%, which indicated that this mode was the dominant factor in the change of the daytime urban thermal environment. We analyzed the modes in both time and space. In time, we analyzed the Pearson correlation between the PC trend in the first mode and the trend in the mean annual LST in the study area. The Pearson correlation coefficient between the PC trend of the first mode and the annual mean LST of the study area was > 0.99 , whereas the other modes tended to be 0. This indicates that the first mode reflects the influence of global effect on the change of thermal environment. The PC of the first mode reflected an upward trend of the daytime thermal environment. In space, all positions of this mode were positive in the EOF, indicating that the global effect was synergistic in the urban daytime thermal environment. The mean EOF values were ranked as urban expansion areas (15.65) $>$ urban renewal areas (12.22) $>$ urban stabilization areas (9.19). This reflects a greater synergy between LST of urban expansion and renewal areas and background climate change. Natural areas had a higher average EOF of 13.92, which was influenced by the specific natural cover. Water bodies and paddy fields showed lower synergy in response to changes in the thermal environment, whereas forests, and dryland-type croplands showed higher synergy. This was also reflected in the mean EOF values of LCZ in the first mode. LCZ 2 and LCZ 5, mid-rise building landscapes that dominate in urban stability and renewal areas, had lower EOF mean values of 11.61, 10.95, respectively, while LCZ 8, large low-rise buildings that dominate urban expansion areas, had higher EOF mean values of 15.61.

The EOF analysis showed that the variance contribution of the second mode was 12.51%, whereas the spatial pattern showed a

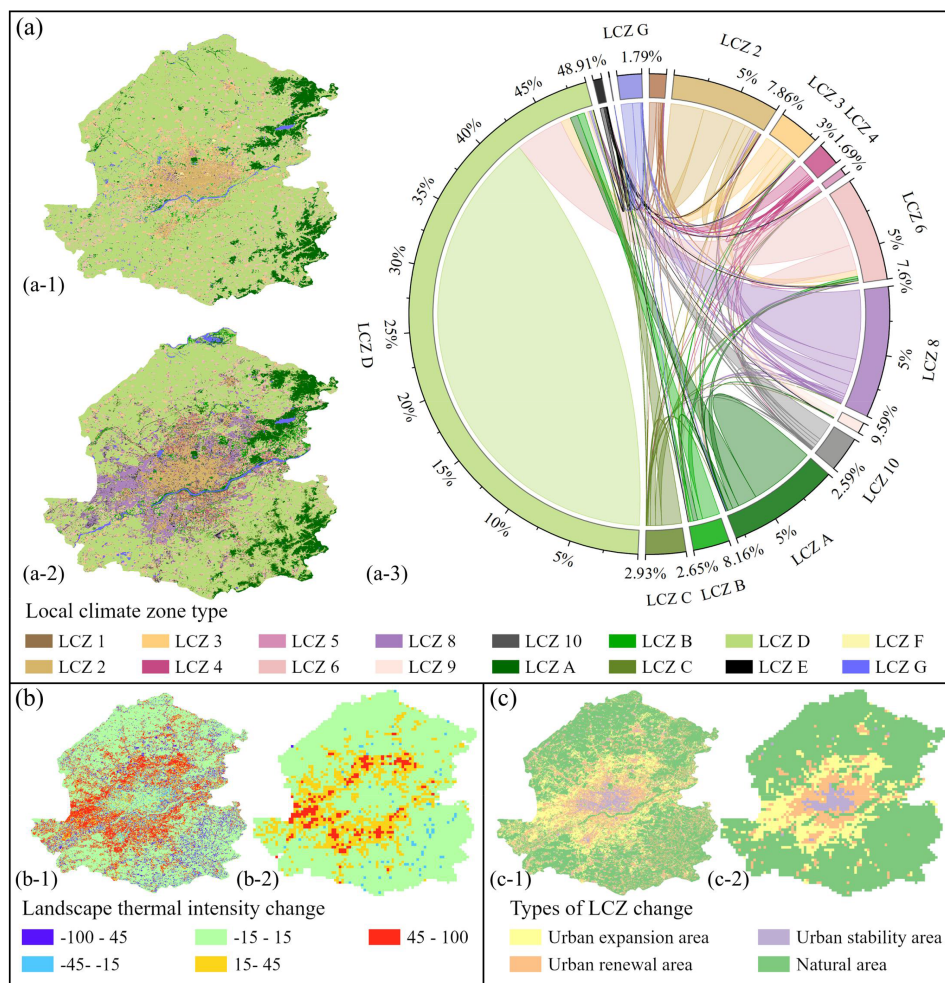


Fig. 3. LCZ evolution and its reflected information. (a) LCZ evolution. (a-1) LCZ in 2000. (a-2) LCZ in 2020. (a-3) dynamic changes. (b) LTI evolution. (b-1) LTI evolution at 100 m resolution. (b-2) LTI evolution at 1000 m resolution. (c) Types of LCZ changes. (c-1) Types of LCZ changes at 100 m resolution. (c-2) Types of LCZ changes at 1000 m resolution.

larger difference between the positive and negative EOF values and a more stable upward trend in PC. In general, the second mode showed a gradual shift from a negative to a positive region, which contributed to a change in the thermal environment. The mean EOF values were ranked as urban expansion areas (15.41) > urban renewal areas (-0.13) > natural areas (-3.85) > urban stabilization areas (-4.13). The EOF values were notably higher in the urban expansion areas than in the other areas. Interestingly, the positive regions produced the same circular distribution pattern as the LTI change. Therefore, this study focused on analyzing the positive regions. Among the positive regions, the EOF values of LCZ 8 (large low-rise buildings), LCZ 10 (heavy industrial zone), and LCZ 1 (compact high-rise buildings) were 19.56, 17.57, 15.89, respectively, which indicated that these three types of landscapes had the most obvious warming effects, whereas the EOF value of LCZ A (dense trees) and LCZ G (water bodies) were 8.29, 9.28, respectively, which indicated that these two natural landscapes had the least obvious warming effects. The results of the bivariate spatial autocorrelation analysis showed that the global Moran's I index of EOF and LTI in the second mode was 0.57, showing a significant positive trend; the other modes were < 0.2, showing a random pattern. Fig. 5

shows the results of the bivariate local spatial autocorrelation analysis. High-high clustering is the phenomenon in which both the EOF value and LTI of the grid and its neighboring cells show significantly higher than average values, and this part of the region had 64.71% of urban expansion areas. The higher proportion of LCZ 1, LCZ 8, and LCZ 10 in the expansion areas also explained their higher average values in the positive part of the EOF2. Low-low clustering is the phenomenon that both the EOF value and LTI of the grid and its neighboring cells showed significantly lower than average values, and this part of the region had 93.71% of natural areas. The higher proportion of LCZ A, LCZ G in the natural areas also explained that they had lower average values in the positive part of the EOF2. High-low outliers and low-high outliers referred to the phenomenon that the EOF values and LTIs of the grid and its neighboring cells appear to be the opposite of high and low. The high-low outliers, i.e., high EOF values and low LTI, were mainly composed of natural areas. The EOF value of this area was significantly lower than that of the urban expansion ring, which represented a methodological error. Low-high outliers, i.e., low EOF values and high LTI. This part of the area was small and mainly distributed at the junction of the urban renewal

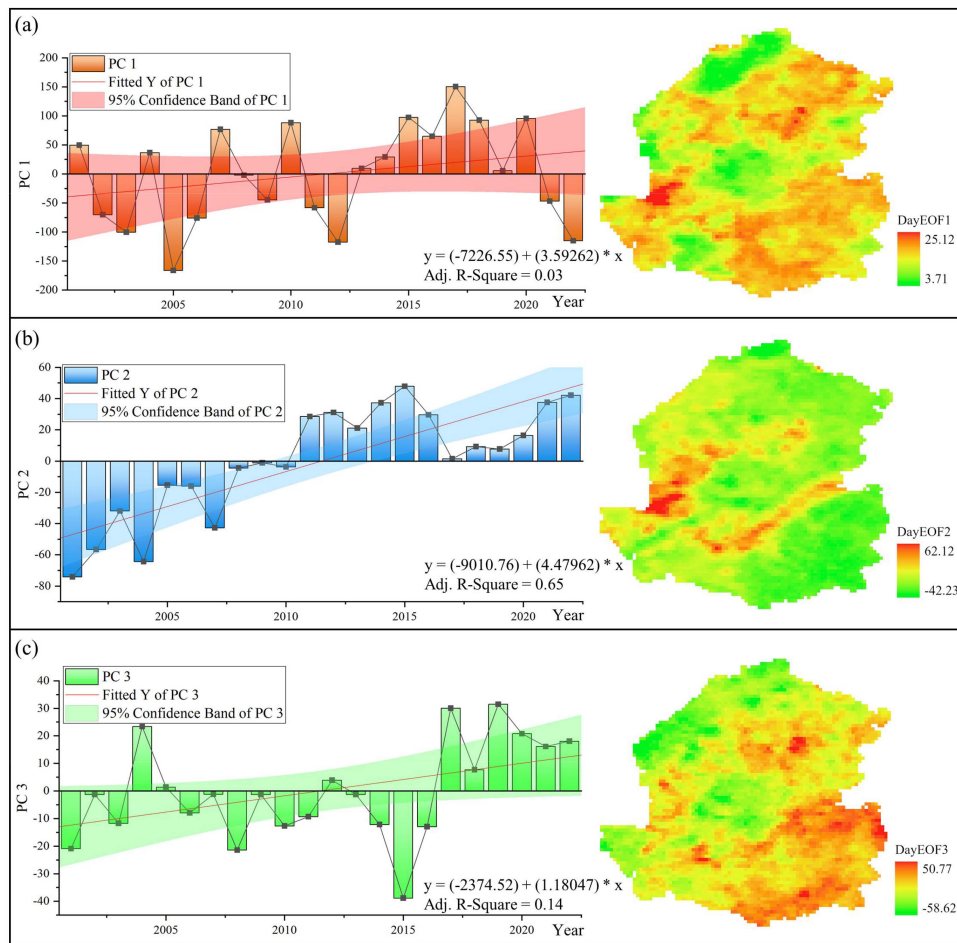


Fig. 4. EOF modes of the daytime thermal environment. (a) First mode. (b) Second mode. (c) Third mode.

area and the expansion area, which might be affected by the edge effect.

In summary, this suggested that the contribution of urban expansion areas to thermal environment variation was higher than that of urban stability, urban renewal area and natural area, mainly because the shift of the landscape from natural to built-up types results in greater changes in subsurface properties, such as heat capacity, heat transfer, and albedo [33], [37], [38]. In Shenyang City, the urban expansion area showed a typical ring-type expansion pattern [39]. This pattern of urban growth makes it easy for cities to plan and manage, but also tends to distribute urban heat islands continuously, deepening their intensity and creating greater thermal health risks for residents during heat waves [40], [41]. Therefore, it is important to be aware of the dangerous effects of this expansion pattern on the local thermal environment [42], [43], [44]. In addition, both LCZ 8 and LCZ 10 have high values in the EOF1 and the positive part of EOF2, indicating that ultrahigh heat emissions from industrial zones have an enhanced effect on surface thermal environment changes over a long time series.

The EOF analysis showed that the variance contribution of the third mode was 3.16%, showing the spatial distribution characteristics of low center—high surrounding similar to that of the first mode. However, there was an evident difference between the positive and negative values of both PC and EOF, indicating

that the effect of the third mode on the thermal environment was heterogeneous at different time points. Specifically, before 2016, urban stabilization and renewal areas, water bodies, and paddy field croplands exerted warming effects on the thermal environment, whereas urban expansion areas, forests, and dryland croplands exerted cooling effects. This trend reversed after 2016. Thus, the third mode revealed a local urbanization effect in urban stabilization and renewal areas mainly in the early part of the study period; the contribution of this mode to thermal environment variation was low.

C. Influencing Factors of Nighttime Thermal Environment Changes

In the deconstruction of the nighttime thermal environment using EOF analysis, the first two modes passed the North test and could explain 85.45% of the variation of the nighttime thermal environment in the study area; their EOF and PC are shown in Fig. 6.

Among them, the EOF analysis showed that the first mode had a variance contribution of 81.33%, and its trend of PC also had a Pearson correlation coefficient of > 0.99 with the trend of annual mean LST in the study area, whereas the trend of PC of the second mode had a Pearson correlation of nearly 0. Therefore, the first mode also reflects the global effect of the

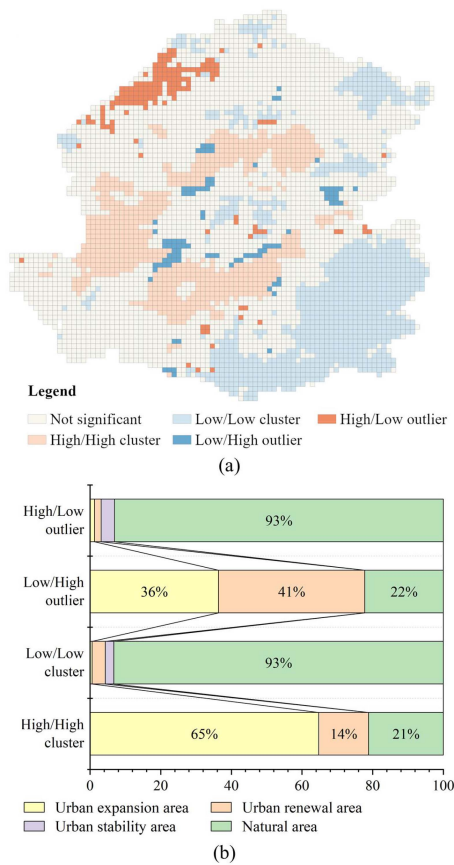


Fig. 5. Results of local bivariate spatial autocorrelation analysis of EOF and LTI in the second mode of the daytime thermal environment. (a) Spatial significance. (b) Composition of significant regions. High-high clustering is the phenomenon in which both the EOF value and LTI of the grid and its neighboring cells show significantly higher than average values. Low-low clustering is the phenomenon that both the EOF value and LTI of the grid and its neighboring cells showed significantly lower than average values. High-low outliers and low-high outliers refer to the phenomenon that the EOF values and LTIs of the grid and its neighboring cells appear to be the opposite of high and low. Not significant is that the EOF values and LTI of the grid and its neighboring cells do not show a significant relationship.

nighttime thermal environment, which is more evidently and singularly influenced by the background climate effect than the daytime thermal environment, and the rising trend is more stable. In space, as with the daytime thermal environment, all spatial locations in the first mode of the nighttime thermal environment were positive, reflecting the synergistic nature of the background climate influence. The mean EOF values were ranked as urban expansion areas (15.48) > urban renewal areas (15.22) > natural areas (13.68) > urban stabilization areas (11.95). Compared to the daytime thermal environment, the nighttime thermal environment had a smaller standard deviation of EOF between areas, suggesting that climate change affects the nighttime thermal environment more uniformly. Several areas of urban expansion, renewal zones, and water bodies had obviously unusually high EOF values, whereas urban stabilization areas and other natural covers had lower EOF values.

The EOF analysis showed that the variance contribution of the second mode was 4.12%. The EOF of the second mode showed a large difference between positive and negative values, whereas the spatial distribution of high and low values showed

the opposite trend to that of the first mode. The mean EOF values were ranked as natural areas (5.42) > urban stabilization areas (-5.28) > urban expansion areas (-9.15) > urban renewal areas (-10.41). Urban expansion and renewal areas had notably lower EOF values. Combined with the PC, the second mode demonstrated a gradual shift in the study area from positive regions, contributing significantly to the thermal environmental change, to unusually prominent negative regions, contributing significantly to thermal environmental change.

In this study, the high-value anomalous regions in the first model and the corresponding low-value anomalous regions in the second model were further analyzed as the regions of interest. If the two modes are considered together, the values of EOF*PC for the two modes in the regions of interest have a positive and negative neutralizing effect before 2012 and a positive and positive superimposing effect after 2012. It is possible that this reflects a change in LTI in the urban expansion area. Therefore, we further used bivariate local spatial autocorrelation analysis to illustrate the role of LTI changes on the formation of the regions of interest, and the results are shown in Fig. 7. The regions of interest were above the mean in the first mode and below the mean in the second mode. Since LTI was higher than the mean if the urban morphology is highly variable, the regions of interest show high-high cluster in EOF 1 and low-high outlier in EOF 2. We extracted the overlapping parts of the two as the regions of interest, and the LCZ transition types and compositions of the regions of interest were counted, as shown in Table II. The remaining regions with clustered or outlier features all had significantly lower absolute EOF values than the region of interest and were therefore not included in the analysis.

The results showed that 64.49% of the regions of interest were urban expansion areas and 23.40% were urban renewal areas. The proportion of high-rise built-up landscapes in the regions of interest exceeded 30%, with the highest EOF values in both modes. This indicated that LCZ 1 and 4 high-rise buildings in the expansion area had the most significant warming effect on the nighttime thermal environment among residential landscapes. In addition, LCZs 2, 5, 8, and 10 also had > 20% share, while low-rise built-up landscapes (LCZ 3, 6, and 9) had a lower share in this area. Formation of the regions of interest may reflect the high thermal emission behavior of the residential landscape at night. Previous studies have shown that this observation varies by city. For example, Sydney, Rio de Janeiro, and Jakarta, where LCZ 1 and 4 high-rise buildings tend to concentrate along waterfronts or in central business districts with large green areas, have lower intensity urban heat island effects [45]. In Shenyang, LCZ 1 in the expansion area is embedded in the surrounding built environment with a high construction intensity, producing a stronger warming effect, similar to the case of Los Angeles. Therefore, it is necessary to pay more attention to the impact of localized overheating phenomenon in middle and high-rise built-up areas in Shenyang.

V. DISCUSSION

A. LCZ Mapping Based on Remote Sensing Workflow

Remote sensing workflow that utilizes exclusively Earth observation data for classification has been widely adopted in

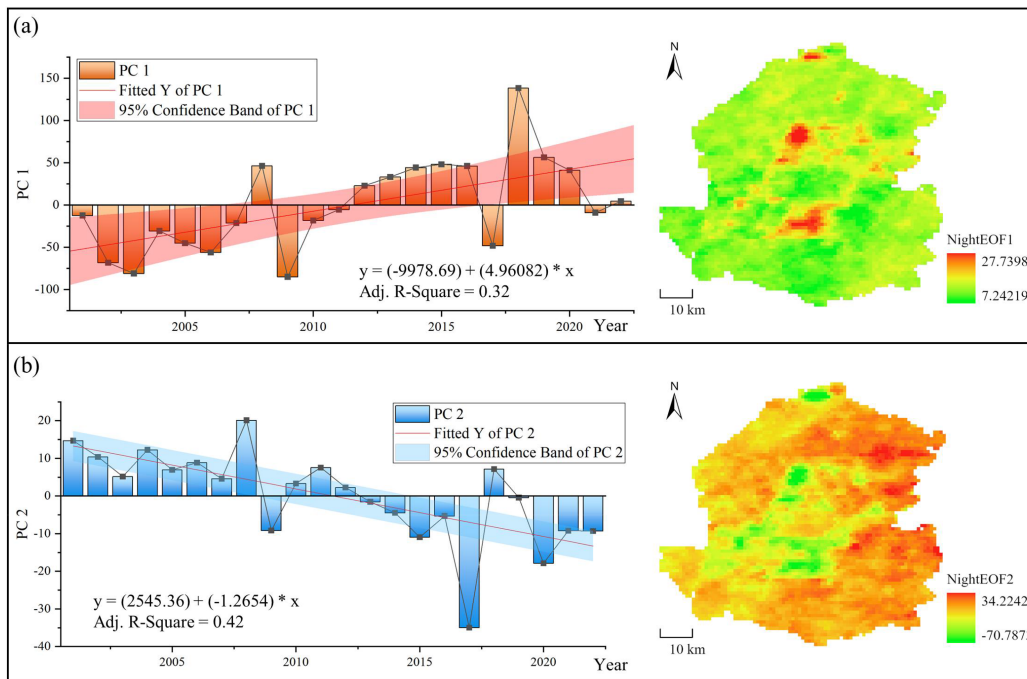


Fig. 6. EOF modes of the nighttime thermal environment. (a) First mode. (b) Second mode.

the LCZ mapping process. In previous studies, convolutional neural networks tend to improve overall accuracy by 6–8% and construct type accuracy by 10–13% compared to random forest methods [46], [47], and are the main development direction for LCZ mapping [48]. On the basis of convolutional neural networks, special networks such as LCZ-NET and MSMLA have been developed for image classification [48], [49]. Some scholars further introduced the object-oriented classification method to classify the very high resolution images and obtained the classification result with 89% accuracy [50], [51]. However, the year of availability of Sentinel 2 image data, which is widely used in convolutional neural networks, is after 2015. This limits the acquisition of urban morphology in long time series. Therefore, the random forest-based LCZ mapping workflow designed by WUDAPT is selected for this study. The WUDAPT process allows earlier Landsat 7 images to be entered for classification. Furthermore, due to its good transfer properties, the process has been widely promoted worldwide [52], [53]. By applying the LCZ concept, this study further explains the differences in the role of 3-D morphology on the thermal environment compared to previous studies focusing on 2-D urban morphology.

B. Application of Adaptation and Mitigation Strategies

The causes of changes in the global thermal environment are complex and have led to its oscillatory nature, showing a general upward trend [12]. Previous studies have used similar signal extraction methods to extract hidden information from oscillatory changes in the thermal environment and have found that once the influence of background climate effects is removed, local factors with urbanization as the main driver cause common features in urban temperatures [24]. This study decomposed the thermal environment into background and perturbation fields using EOF

at the urban scale [22], further confirming that the contribution of global effect to urban thermal environment change is much larger than that of local effects, especially at night. This will help to better understand the impacts of background climate change and urbanization on the urban thermal environment so that mitigation and adaptation strategies can be better targeted.

The core objective of this mitigation strategy is to reduce carbon emissions and increase carbon sinks to slow the warming rate of the background climate [54]. This study demonstrates that background climate effects are the dominant factors in thermal environmental change and that mitigation measures can fundamentally reduce the adverse effects of thermal environmental change. The main expansion type in Shenyang in recent years has been LCZ 8, which is dominated by industrial land use, and it is important to reduce fossil fuel use, improve energy efficiency, and promote clean energy to reduce carbon emissions [55], [56], [57]. At the same time, a large amount of agricultural land LCZ D exists in Shenyang, and there is a need to focus on GHS emissions caused by soil management, fertilizer use, and rice cultivation in the land system [58], [59].

This study demonstrated that urban sprawl behavior can have a significant impact on thermal environmental change, and the intensity of the effect at the local scale is even higher than that of the background climate effect [60]. Owing to urban development and historical emission problems, changes in the thermal environment are inevitable in the future. [61]. Therefore, adaptation to changes in the thermal environment must be enhanced on a local scale [62]. Nature-based solutions have become a hot topic of international interest following the UN Summit in New York in September 2019 [63]. In the field of urban planning and management, the program emphasizes the important role of nature-based approaches, such as afforestation and ecological restoration, in regulating the urban climate. This approach is

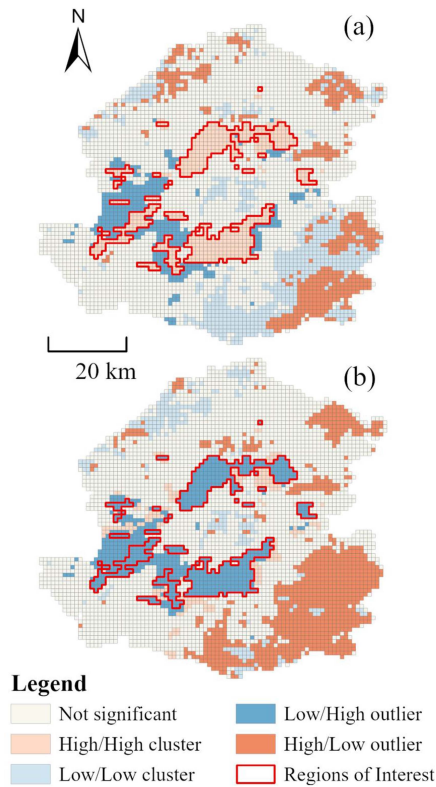


Fig. 7. Results of bivariate local spatial autocorrelation analysis of nighttime EOF and LTI. (a) First mode. (b) Second mode. We focused on the association of the anomalous part with LTI in the EOF of both modalities. The anomalies are shown as high values in the first mode and low values in the second mode, and high values for large changes in LTI. Therefore, the anomalies are shown as high-high cluster in the first mode and high-low outlier in the second mode, and the overlap of the two is considered as the region of interest. Other types of spatial autocorrelation are not obvious on the EOF of the nighttime mode, so they are not analyzed.

characterized by low energy consumption, high sustainability, and flexibility compared with active adaptation strategies, such as air conditioning [64], [65], [66]. In built-up industrial and mid-rise building areas, the thermal environment can be improved by planting street trees to increase vegetation or by promoting green façades and roofs [67], [68], [69]. Among the emerging expansion areas, attention should be paid to the construction of urban parks [70], [71]. The design and planning of ventilation and ecological corridors on a macroscopic scale to create connections with cold-source areas can play an effective role in cooling by improving the efficiency of air circulation in areas of high construction density [72], [73]. Moreover, existing studies have shown that the knowledge level of high-temperature adaptation is lower among the elderly, less educated, and unhealthy groups [74]. Therefore, providing citizens with knowledge to adapt to changes in the thermal environment through sound policies, social and economic support also plays an important role [75].

C. Limitations

This study provides a novel perspective to clarify the global-local causes of urban diurnal thermal environment changes.

However, the EOF method is more subjective, so the results may vary in different cities. In subsequent studies, further expansion of the study cities is needed to analyze the stability of the results and ways to improve them.

V. CONCLUSION

Based on the LST and LCZ datasets for a long time series, this study explored the contribution of background climate effects and local effects to changes in the thermal environment in Shenyang City using correlation analysis and bivariate spatial autocorrelation analysis, and explained the warming effect of the landscape on the thermal environment. The main conclusions are as follows:

- 1) Background climate significantly contributes to the thermal environment. The correlation coefficient between the PC of the first mode and mean LST was > 0.99 , reflecting the daytime background temperature trend. The effect of background climate is generally reflected in time as a warming effect, with the warming effect of the daytime thermal environment being more oscillatory, whereas the nighttime thermal environment is smoother. Spatially, the urban expansion area is more synergistic with changes in the background climate effect, whereas the urban stabilization and renewal areas shows lower synergy.
- 2) Urban expansion makes a secondary contribution to the thermal environment. This study shows that the EOF of the second mode has a clear spatial correlation with LTI change, forming a circular zone of synergistic change during the daytime and multiple outlier prominent areas at night, reflecting the local landscape and urbanization effects brought about by urban expansion and renewal. The PC of the second mode had a more obvious single change trend, and the turning point of the PC sign was in around 2010, indicating that suburban sprawl behavior contributed to thermal environment change after 2010.
- 3) Among the expansion and renewal zones, the industrial landscape represented by LCZ 8 large low-rise and LCZ 10 heavy industrial zones, and the compact high-rise landscape LCZ 1 had the most obvious warming effect on the daytime thermal environment, which may be due to the synergistic effect of the local landscape effect generated by daytime radiative forcing and the high heat emission from the industrial zone. The compact mid-rise buildings represented by LCZ 1, 2, 4, and 5 had the most obvious warming effect on the nighttime thermal environment, which may be due to high heat emissions at night, mainly concentrated in high-density residential areas.

The results of this study demonstrate the need to exploit the synergy between global mitigation and local adaptation strategies. In Shenyang City, there is a need to emphasize the mitigation role of industrial and agricultural areas through energy conservation and emission reduction measures, and to focus on nature-based solutions to enhance adaptive capacity in urban expansion areas.

APPENDIX

TABLE III
DEFINITION, REAL SCENE, AND PARAMETERS OF LCZ

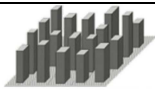



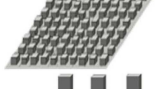

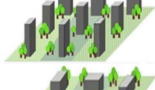

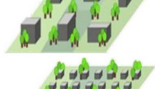

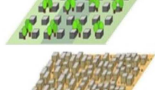

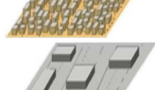


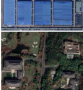


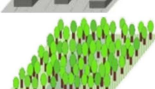

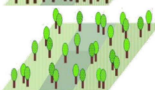



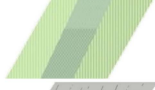
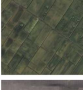


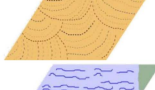


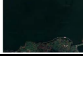


LCZ types	Illustration of LCZs	Real scene	Building density	Percentage of impervious surface	
LCZ 1 Compact high-rise			40–60	40–60	25–75
LCZ 2 Compact middle-rise			40–70	30–50	10–25
LCZ 3 Compact low-rise			40–70	20–50	3–10
LCZ 4 Open high-rise			20–40	30–40	25–75
LCZ 5 Open middle-rise			20–40	30–50	10–25
LCZ 6 Open low-rise			20–40	20–50	3–10
LCZ 7 Lightweight low-rise			60–90	< 20	2–4
LCZ 8 Large low-rise			30–50	40–50	3–10
LCZ 9 Sparsely built			10–20	< 20	3–10
LCZ 10 Heavy industry			20–30	20–40	5–15
LCZ A Dense tree			<10	<10	0
LCZ B Scattered tree			<10	<10	0
LCZ C Bush, scrub			<10	<10	0
LCZ D Low plants			<10	<10	0
LCZ E Bare rock or paved			<10	<10	0
LCZ F Bare soil or sand			<10	<10	0
LCZ G Water			<10	<10	0

TABLE IV
DATA SOURCES AND DESCRIPTIONS

Data type	Data source	Describe	Resolution	Date
LST	https://earthengine.google.com/	MODIS LST product (MOD11A1)	1000 m	2001–2022 Jun. 1 –Aug. 31 Daytime and nighttime
LCZ	https://www.gscloud.cn/	Landsat 7 ETM Band 1-8 Landsat 8 OLI TIRS Band 1-11	30 m 30 m	2000.09.25 2020.10.10

TABLE V
ACCURACY EVALUATION OF LCZ MAPPING RESULTS

LCZ Type	2000		2020	
	Users. (%)	prod. (%)	Users. (%)	prod. (%)
LCZ1	70.45	50.82	83.93	78.99
LCZ2	65.05	77.01	70.97	77.19
LCZ3	71.68	70.43	53.23	46.48
LCZ4	64.71	24.44	85.33	65.98
LCZ5	66.67	65.12	66.32	67.74
LCZ6	70.78	77.30	61.90	61.18
LCZ8	63.95	66.27	73.91	83.33
LCZ9	68.42	56.52	60.00	45.00
LCZ10	65.82	71.23	73.74	74.49
LCZA	70.63	80.16	70.59	79.34
LCZB	73.86	65.00	76.53	69.44
LCZC	63.27	67.39	59.55	63.10
LCZD	82.40	85.71	71.24	76.76
LCZE	66.04	61.40	63.79	62.71
LCZF	75.64	67.05	64.15	55.74
LCZG	63.27	86.11	76.62	89.39
Overall accuracy(%)	70.75		70.75	
Kappa coefficient	0.6824		0.6861	

REFERENCES

- [1] IPCC, "Summary for policymakers — Global warming of 1.5 °C," 2015. Accessed: Feb. 08, 2023. [Online]. Available: <https://www.ipcc.ch/sr15/chapter/spm/>
- [2] D. Welsby, J. Price, S. Pye, and P. Ekins, "Unextractable fossil fuels in a 1.5°C world," *Nature*, vol. 597, Sep. 2021, Art. no. 7875, doi: [10.1038/s41586-021-03821-8](https://doi.org/10.1038/s41586-021-03821-8).
- [3] L. Wang et al., "Urban warming increases the temperature sensitivity of spring vegetation phenology at 292 cities across China," *Sci. Total Environ.*, vol. 834, Aug. 2022, Art. no. 155154, doi: [10.1016/j.scitotenv.2022.155154](https://doi.org/10.1016/j.scitotenv.2022.155154).
- [4] United Nations, *THE 17 GOALS | Sustainable Development*. New York, NY, USA: USA, 2015.
- [5] W. P. Lowry, "Empirical estimation of urban effects on climate: A problem analysis," *J. Appl. Meteorol. Climatol.*, vol. 16, no. 2, pp. 129–135, 1977.
- [6] Y. He, G. Jia, Y. Hu, and Z. Zhou, "Detecting urban warming signals in climate records," *Adv. Atmos. Sci.*, vol. 30, no. 4, pp. 1143–1153, Jul. 2013, doi: [10.1007/s00376-012-2135-3](https://doi.org/10.1007/s00376-012-2135-3).
- [7] G.-Y. Ren, "Urbanization as a major driver of urban climate change," *Advances in Climate Change Research*, May 2017, Accessed: Jun. 23, 2023. [Online]. Available: https://www.scipedia.com/public/Ren_2015a
- [8] A. Dewan, G. Kiselev, and D. Botje, "Diurnal and seasonal trends and associated determinants of surface urban heat islands in large Bangladesh cities," *Appl. Geogr.*, vol. 135, Oct. 2021, Art. no. 102533, doi: [10.1016/j.apgeog.2021.102533](https://doi.org/10.1016/j.apgeog.2021.102533).
- [9] Z. Shen, J. Shi, J. Tan, and H. Yang, "The migration of the warming center and urban heat island effect in shanghai during urbanization," *Front. Earth Sci.*, vol. 8, Aug. 2020, Art. no. 25014, doi: [10.3389/feart.2020.00340](https://doi.org/10.3389/feart.2020.00340).
- [10] V. K. Singh, S. Bhati, M. Mohan, N. R. Sahoo, and S. Dash, "Numerical simulation of the impact of urban canopies and anthropogenic emissions on heat island effect in an industrial area: A case study of Angul–Talcher region in India," *Atmospheric Res.*, vol. 277, Oct. 2022, Art. no. 106320, doi: [10.1016/j.atmosres.2022.106320](https://doi.org/10.1016/j.atmosres.2022.106320).
- [11] N. Skarbit, I. D. Stewart, J. Unger, and T. Gál, "Employing an urban meteorological network to monitor air temperature conditions in the 'local climate zones' of szeged, Hungary," *Int. J. Climatol.*, vol. 37, no. S1, pp. 582–596, 2017, doi: [10.1002/joc.5023](https://doi.org/10.1002/joc.5023).
- [12] Z. Liu et al., "Surface warming in global cities is substantially more rapid than in rural background areas," *Commun. Earth Environ.*, vol. 3, no. 1, Sep. 2022, Art. no. 1, doi: [10.1038/s43247-022-00539-x](https://doi.org/10.1038/s43247-022-00539-x).
- [13] A. Guo, W. Yue, J. Yang, T. He, M. Zhang, and M. Li, "Divergent impact of urban 2D/3D morphology on thermal environment along urban gradients," *Urban Climate*, vol. 45, Sep. 2022, Art. no. 101278, doi: [10.1016/j.uclim.2022.101278](https://doi.org/10.1016/j.uclim.2022.101278).
- [14] A. Guo et al., "Impact of urban morphology and landscape characteristics on spatiotemporal heterogeneity of land surface temperature," *Sustain. Cities Soc.*, vol. 63, Dec. 2020, Art. no. 102443, doi: [10.1016/j.scs.2020.102443](https://doi.org/10.1016/j.scs.2020.102443).
- [15] A. Guo, J. Yang, X. Xiao, C. J. Xia, and X. Li, "Influences of urban spatial form on urban heat island effects at the community level in China," *Sustain. Cities Soc.*, vol. 53, Feb. 2020, Art. no. 101972, doi: [10.1016/j.scs.2019.101972](https://doi.org/10.1016/j.scs.2019.101972).
- [16] Y. Liu, X. Huang, Q. Yang, and Y. Cao, "The turning point between urban vegetation and artificial surfaces for their competitive effect on land surface temperature," *J. Cleaner Prod.*, vol. 292, Apr. 2021, Art. no. 126034, doi: [10.1016/j.jclepro.2021.126034](https://doi.org/10.1016/j.jclepro.2021.126034).

- [17] J. Peng, J. Jia, Y. Liu, H. Li, and J. Wu, "Seasonal contrast of the dominant factors for spatial distribution of land surface temperature in urban areas," *Remote Sens. Environ.*, vol. 215, pp. 255–267, Sep. 2018, doi: [10.1016/j.rse.2018.06.010](https://doi.org/10.1016/j.rse.2018.06.010).
- [18] Z. Cai, Y. Tang, and Q. Zhan, "A cooled city? Comparing human activity changes on the impact of urban thermal environment before and after city-wide lockdown," *Building Environ.*, vol. 195, May 2021, Art. no. 107729, doi: [10.1016/j.buildenv.2021.107729](https://doi.org/10.1016/j.buildenv.2021.107729).
- [19] M. Latif, J. Sun, M. Visbeck, and M. Hadi Bordbar, "Natural variability has dominated Atlantic meridional overturning circulation since 1900," *Nature Climate Change*, vol. 12, no. 5, May 2022, Art. no. 5, doi: [10.1038/s41558-022-01342-4](https://doi.org/10.1038/s41558-022-01342-4).
- [20] F. Pöppelmeier, A. Jeltsch-Thömmes, J. Lippold, F. Joos, and T. F. Stocker, "Multi-proxy constraints on Atlantic circulation dynamics since the last ice age," *Nature Geosci.*, vol. 16, no. 4, Apr. 2023, Art. no. 4, doi: [10.1038/s41561-023-01140-3](https://doi.org/10.1038/s41561-023-01140-3).
- [21] M. Bhattacharya and M. Sinha, "Basin scale wind-wave prediction using empirical orthogonal function analysis and neural network models," *Results Geophysical Sci.*, vol. 8, Dec. 2021, Art. no. 100032, doi: [10.1016/j.ringsps.2021.100032](https://doi.org/10.1016/j.ringsps.2021.100032).
- [22] L. Ren et al., "Investigations into mode characteristics of wind fields off the Guangdong coast using empirical orthogonal function," *Energy Rep.*, vol. 8, pp. 202–211, Dec. 2022, doi: [10.1016/j.egy.2022.11.004](https://doi.org/10.1016/j.egy.2022.11.004).
- [23] Y. Ma, H. Yang, Z. Deng, Y. Qin, J. Li, and X. Wei, "Intra-seasonal variability of autumn rainfall in the Yangtze river delta and its related atmospheric circulations," *Atmospheric Res.*, vol. 278, Nov. 2022, Art. no. 106363, doi: [10.1016/j.atmosres.2022.106363](https://doi.org/10.1016/j.atmosres.2022.106363).
- [24] F. Estrada and P. Perron, "Disentangling the trend in the warming of urban areas into global and local factors," *Ann. New York Acad. Sci.*, vol. 1504, no. 1, pp. 230–246, 2021, doi: [10.1111/myas.14691](https://doi.org/10.1111/myas.14691).
- [25] K. Liu, H. Su, X. Li, W. Wang, L. Yang, and H. Liang, "Quantifying spatial-temporal pattern of urban heat island in Beijing: An improved assessment using land surface temperature (LST) time series observations from LANDSAT, MODIS, and Chinese new satellite GaoFen-1," *IEEE J. Sel. Topics Appl. Earth Observ. Remote Sens.*, vol. 9, no. 5, pp. 2028–2042, May 2016, doi: [10.1109/JSTARS.2015.2513598](https://doi.org/10.1109/JSTARS.2015.2513598).
- [26] S. Bonafoni, "Downscaling of landsat and MODIS land surface temperature over the heterogeneous urban area of Milan," *IEEE J. Sel. Topics Appl. Earth Observ. Remote Sens.*, vol. 9, no. 5, pp. 2019–2027, May 2016, doi: [10.1109/JSTARS.2016.2514367](https://doi.org/10.1109/JSTARS.2016.2514367).
- [27] S. A. Nowicki, "Thermophysical characterization of the southwestern U.S. from 5 years of MODIS land surface temperature observations," *IEEE J. Sel. Topics Appl. Earth Observ. Remote Sens.*, vol. 7, no. 8, pp. 3416–3420, Aug. 2014, doi: [10.1109/JSTARS.2014.2349001](https://doi.org/10.1109/JSTARS.2014.2349001).
- [28] J. Yu et al., "Interannual spatiotemporal variations of land surface temperature in China from 2003 to 2018," *IEEE J. Sel. Topics Appl. Earth Observ. Remote Sens.*, vol. 14, pp. 1783–1795, 2021, doi: [10.1109/JSTARS.2020.3048823](https://doi.org/10.1109/JSTARS.2020.3048823).
- [29] S.-B. Duan, C. Huang, X. Liu, M. Liu, Y. Sun, and C. Gao, "Spatio-temporal distribution characteristics of global annual maximum land surface temperature derived from MODIS thermal infrared data from 2003 to 2019," *IEEE J. Sel. Topics Appl. Earth Observ. Remote Sens.*, vol. 15, pp. 4690–4697, 2022, doi: [10.1109/JSTARS.2022.3181051](https://doi.org/10.1109/JSTARS.2022.3181051).
- [30] I. D. Stewart and T. R. Oke, "Local climate zones for urban temperature studies," *Bull. Amer. Meteorological Soc.*, vol. 93, no. 12, pp. 1879–1900, Dec. 2012, doi: [10.1175/BAMS-D-11-00019.1](https://doi.org/10.1175/BAMS-D-11-00019.1).
- [31] J. Yang, Y. Wang, C. Xiu, X. Xiao, J. Xia, and C. Jin, "Optimizing local climate zones to mitigate urban heat island effect in human settlements," *J. Cleaner Prod.*, vol. 275, Dec. 2020, Art. no. 123767, doi: [10.1016/j.jclepro.2020.123767](https://doi.org/10.1016/j.jclepro.2020.123767).
- [32] J. Ren et al., "Exploring thermal comfort of urban buildings based on local climate zones," *J. Cleaner Prod.*, vol. 340, Mar. 2022, Art. no. 130744, doi: [10.1016/j.jclepro.2022.130744](https://doi.org/10.1016/j.jclepro.2022.130744).
- [33] J. Yang et al., "Understanding land surface temperature impact factors based on local climate zones," *Sustain. Cities Soc.*, vol. 69, Jun. 2021, Art. no. 102818, doi: [10.1016/j.scs.2021.102818](https://doi.org/10.1016/j.scs.2021.102818).
- [34] J. Xie, C. Ren, X. Li, and L. C. H. Chung, "Investigate the urban growth and urban-rural gradients based on local climate zones (1999–2019) in the greater bay area, China," *Remote Sens. Appl., Soc. Environ.*, vol. 25, Jan. 2022, Art. no. 100669, doi: [10.1016/j.rsase.2021.100669](https://doi.org/10.1016/j.rsase.2021.100669).
- [35] W. Ji, Y. Chen, K. Li, and X. Dai, "Multicascaded feature fusion-based deep learning network for local climate zone classification based on the So2Sat LCZ42 benchmark dataset," *IEEE J. Sel. Topics Appl. Earth Observ. Remote Sens.*, vol. 16, pp. 449–467, 2023, doi: [10.1109/JSTARS.2022.3226524](https://doi.org/10.1109/JSTARS.2022.3226524).
- [36] B. Bechtel et al., "Generating WUDAPT level 0 data—Current status of production and evaluation," *Urban Climate*, vol. 27, pp. 24–45, Mar. 2019, doi: [10.1016/j.uclim.2018.10.001](https://doi.org/10.1016/j.uclim.2018.10.001).
- [37] J. Ren, J. Yang, F. Wu, W. Sun, X. Xiao, and J. Xia, "Regional thermal environment changes: Integration of satellite data and land use/land cover," *iScience*, vol. 9, Dec. 2022, Art. no. 105820, doi: [10.1016/j.isci.2022.105820](https://doi.org/10.1016/j.isci.2022.105820).
- [38] W. Yu et al., "Downscaling mapping method for local climate zones from the perspective of deep learning," *Urban Climate*, vol. 49, May 2023, Art. no. 101500, doi: [10.1016/j.uclim.2023.101500](https://doi.org/10.1016/j.uclim.2023.101500).
- [39] Y. Zheng, Y. He, Q. Zhou, and H. Wang, "Quantitative evaluation of urban expansion using NPP-VIIRS nighttime light and landsat spectral data," *Sustain. Cities Soc.*, vol. 76, Jan. 2022, Art. no. 103338, doi: [10.1016/j.scs.2021.103338](https://doi.org/10.1016/j.scs.2021.103338).
- [40] G. Chen, Y. Chen, H. He, J. Wang, L. Zhao, and Y. Cai, "Assessing the synergies between heat waves and urban heat islands of different local climate zones in Guangzhou, China," *Building Environ.*, vol. 240, Jul. 2023, Art. no. 110434, doi: [10.1016/j.buildenv.2023.110434](https://doi.org/10.1016/j.buildenv.2023.110434).
- [41] M. Milelli, F. Bassani, V. Garbero, D. Poggi, J. von Hardenberg, and L. Riboldi, "Characterization of the urban heat and dry island effects in the Turin metropolitan area," *Urban Climate*, vol. 47, Jan. 2023, Art. no. 101397, doi: [10.1016/j.uclim.2022.101397](https://doi.org/10.1016/j.uclim.2022.101397).
- [42] G. Rahman, N. H. Chandio, M. F. Ul Moazzam, and N. Al Ansari, "Urban expansion impacts on agricultural land and thermal environment in Larkana, Pakistan," *Front. Environ. Sci.*, vol. 11, Mar. 2023, Art. no. 1115553, doi: [10.3389/fenvs.2023.1115553](https://doi.org/10.3389/fenvs.2023.1115553).
- [43] P. Tian et al., "Assessing spatiotemporal characteristics of urban heat islands from the perspective of an urban expansion and green infrastructure," *Sustain. Cities Soc.*, vol. 74, Nov. 2021, Art. no. 103208, doi: [10.1016/j.scs.2021.103208](https://doi.org/10.1016/j.scs.2021.103208).
- [44] Z. Yang, Y. Chen, and Z. Wu, "How urban expansion affects the thermal environment? A study of the impact of natural cities on the thermal field value and footprint of thermal environment," *Ecological Indicators*, vol. 126, Jul. 2021, Art. no. 107632, doi: [10.1016/j.ecolind.2021.107632](https://doi.org/10.1016/j.ecolind.2021.107632).
- [45] B. Bechtel et al., "SUHI analysis using Local climate zones—A comparison of 50 cities," *Urban Climate*, vol. 28, Jun. 2019, Art. no. 100451, doi: [10.1016/j.uclim.2019.01.005](https://doi.org/10.1016/j.uclim.2019.01.005).
- [46] C. Qiu, L. Liebel, L. H. Hughes, M. Schmitt, M. Körner, and X. X. Zhu, "Multitask learning for human settlement extent regression and local climate zone classification," *IEEE Geosci. Remote Sens. Lett.*, vol. 19, 2022, Art. no. 1000705, doi: [10.1109/LGRS.2020.3037246](https://doi.org/10.1109/LGRS.2020.3037246).
- [47] C. Yoo, D. Han, J. Im, and B. Bechtel, "Comparison between convolutional neural networks and random forest for local climate zone classification in mega urban areas using landsat images," *ISPRS J. Photogrammetry Remote Sens.*, vol. 157, pp. 155–170, Nov. 2019, doi: [10.1016/j.isprsjprs.2019.09.009](https://doi.org/10.1016/j.isprsjprs.2019.09.009).
- [48] S. Liu and Q. Shi, "Local climate zone mapping as remote sensing scene classification using deep learning: A case study of metropolitan China," *ISPRS J. Photogrammetry Remote Sens.*, vol. 164, pp. 229–242, Jun. 2020, doi: [10.1016/j.isprsjprs.2020.04.008](https://doi.org/10.1016/j.isprsjprs.2020.04.008).
- [49] M. Kim, D. Jeong, and Y. Kim, "Local climate zone classification using a multi-scale, multi-level attention network," *ISPRS J. Photogrammetry Remote Sens.*, vol. 181, pp. 345–366, Nov. 2021, doi: [10.1016/j.isprsjprs.2021.09.015](https://doi.org/10.1016/j.isprsjprs.2021.09.015).
- [50] G. Chen, Q. Weng, G. J. Hay, and Y. He, "Geographic object-based image analysis (GEOBIA): Emerging trends and future opportunities," *GIScience Remote Sens.*, vol. 55, no. 2, pp. 159–182, Mar. 2018, doi: [10.1080/15481603.2018.1426092](https://doi.org/10.1080/15481603.2018.1426092).
- [51] R. M. Simanjuntak, M. Kuffer, and D. Reckien, "Object-based image analysis to map local climate zones: The case of Bandung, Indonesia," *Appl. Geogr.*, vol. 106, pp. 108–121, May 2019, doi: [10.1016/j.apgeog.2019.04.001](https://doi.org/10.1016/j.apgeog.2019.04.001).
- [52] M. Demuzere, B. Bechtel, A. Middel, and G. Mills, "Mapping Europe into local climate zones," *PLoS One*, vol. 14, no. 4, Apr. 2019, Art. no. e0214474, doi: [10.1371/journal.pone.0214474](https://doi.org/10.1371/journal.pone.0214474).
- [53] M. Demuzere, S. Hankey, G. Mills, W. Zhang, T. Lu, and B. Bechtel, "Combining expert and crowd-sourced training data to map urban form and functions for the continental US," *Sci. Data*, vol. 7, no. 1, Aug. 2020, Art. no. 1, doi: [10.1038/s41597-020-00605-z](https://doi.org/10.1038/s41597-020-00605-z).
- [54] Z. Liu et al., "Challenges and opportunities for carbon neutrality in China," *Nature Rev. Earth Environ.*, vol. 3, no. 2, Feb. 2022, Art. no. 2, doi: [10.1038/s43017-021-00244-x](https://doi.org/10.1038/s43017-021-00244-x).
- [55] Y. Lin, L. Ma, Z. Li, and W. Ni, "The carbon reduction potential by improving technical efficiency from energy sources to final services in China: An extended kaya identity analysis," *Energy*, vol. 263, Jan. 2023, Art. no. 125963, doi: [10.1016/j.energy.2022.125963](https://doi.org/10.1016/j.energy.2022.125963).

- [56] Z. Liu et al., "Reduced carbon emission estimates from fossil fuel combustion and cement production in China," *Nature*, vol. 524, Aug. 2015, Art. no. 7565, doi: [10.1038/nature14677](https://doi.org/10.1038/nature14677).
- [57] X. Teng, W. Zhuang, F. Liu, T. Chang, and Y. Chiu, "China's path of carbon neutralization to develop green energy and improve energy efficiency," *Renewable Energy*, vol. 206, pp. 397–408, Apr. 2023, doi: [10.1016/j.renene.2023.01.104](https://doi.org/10.1016/j.renene.2023.01.104).
- [58] S. C. Cook-Patton et al., "Protect, manage and then restore lands for climate mitigation," *Nature Climate Change*, vol. 11, no. 12, Dec. 2021, Art. no. 12, doi: [10.1038/s41558-021-01198-0](https://doi.org/10.1038/s41558-021-01198-0).
- [59] F. Humpeöder et al., "Overcoming global inequality is critical for land-based mitigation in line with the Paris agreement," *Nature Commun.*, vol. 13, no. 1, Dec. 2022, Art. no. 1, doi: [10.1038/s41467-022-35114-7](https://doi.org/10.1038/s41467-022-35114-7).
- [60] Z. Qiao, T. He, Y. Lu, Y. Sun, X. Xu, and J. Yang, "Quantifying the contribution of land use change based on the effects of global climate change and human activities on urban thermal environment in the Beijing–Tianjin–Hebei urban agglomeration," *Geographical Res.*, vol. 41, no. 7, pp. 1932–1947, 2022.
- [61] M. Roelfsema et al., "Taking stock of national climate policies to evaluate implementation of the Paris agreement," *Nature Commun.*, vol. 11, no. 1, Apr. 2020, Art. no. 1, doi: [10.1038/s41467-020-15414-6](https://doi.org/10.1038/s41467-020-15414-6).
- [62] L. Shi and S. Moser, "Transformative climate adaptation in the United States: Trends and prospects," *Science*, vol. 372, no. 6549, Jun. 2021, Art. no. eabc8054, doi: [10.1126/science.abc8054](https://doi.org/10.1126/science.abc8054).
- [63] United Nations, "Nature-based solutions for climate," *UNEP—UN Environment Programme*, Apr. 16, 2019. Accessed: Jun. 16, 2023. [Online]. Available: <http://www.unep.org/nature-based-solutions-climate>
- [64] M. Jain and H. Rohrer, "Assessing transformative change of infrastructures in urban area redevelopments," *Cities*, vol. 124, May 2022, Art. no. 103573, doi: [10.1016/j.cities.2022.103573](https://doi.org/10.1016/j.cities.2022.103573).
- [65] T. Oakes, "Happy town: Cultural governance and biopolitical urbanism in China," *Environ. Plan. A*, vol. 51, no. 1, pp. 244–262, Feb. 2019, doi: [10.1177/0308518X17693621](https://doi.org/10.1177/0308518X17693621).
- [66] W. Zheng, G. Q. Shen, H. Wang, J. Hong, and Z. Li, "Decision support for sustainable urban renewal: A multi-scale model," *Land Use Policy*, vol. 69, pp. 361–371, Dec. 2017, doi: [10.1016/j.landusepol.2017.09.019](https://doi.org/10.1016/j.landusepol.2017.09.019).
- [67] J. Dong et al., "Quantitative study on the cooling effect of green roofs in a high-density urban area—A case study of Xiamen, China," *J. Cleaner Prod.*, vol. 255, May 2020, Art. no. 120152, doi: [10.1016/j.jclepro.2020.120152](https://doi.org/10.1016/j.jclepro.2020.120152).
- [68] B. Zhang, G. Xie, J. Gao, and Y. Yang, "The cooling effect of urban green spaces as a contribution to energy-saving and emission-reduction: A case study in Beijing, China," *Building Environ.*, vol. 76, pp. 37–43, Jun. 2014, doi: [10.1016/j.buildenv.2014.03.003](https://doi.org/10.1016/j.buildenv.2014.03.003).
- [69] C. Bartesaghi Koc, P. Osmond, and A. Peters, "Evaluating the cooling effects of green infrastructure: A systematic review of methods, indicators and data sources," *Sol. Energy*, vol. 166, pp. 486–508, May 2018, doi: [10.1016/j.solener.2018.03.008](https://doi.org/10.1016/j.solener.2018.03.008).
- [70] X. Geng, Z. Yu, D. Zhang, C. Li, Y. Yuan, and X. Wang, "The influence of local background climate on the dominant factors and threshold-size of the cooling effect of urban parks," *Sci. Total Environ.*, vol. 823, Jun. 2022, Art. no. 153806, doi: [10.1016/j.scitotenv.2022.153806](https://doi.org/10.1016/j.scitotenv.2022.153806).
- [71] Y. Zhou et al., "Studies on urban park cooling effects and their driving factors in China: Considering 276 cities under different climate zones," *Building Environ.*, vol. 222, Aug. 2022, Art. no. 109441, doi: [10.1016/j.buildenv.2022.109441](https://doi.org/10.1016/j.buildenv.2022.109441).
- [72] J. Yang et al., "Local climate zone ventilation and urban land surface temperatures: Towards a performance-based and wind-sensitive planning proposal in megacities," *Sustain. Cities Soc.*, vol. 47, May 2019, Art. no. 101487, doi: [10.1016/j.scs.2019.101487](https://doi.org/10.1016/j.scs.2019.101487).
- [73] J. Yang et al., "Contribution of urban ventilation to the thermal environment and urban energy demand: Different climate background perspectives," *Sci. Total Environ.*, vol. 795, Nov. 2021, Art. no. 148791, doi: [10.1016/j.scitotenv.2021.148791](https://doi.org/10.1016/j.scitotenv.2021.148791).
- [74] B.-J. He, W. Wang, A. Sharifi, and X. Liu, "Progress, knowledge gap and future directions of urban heat mitigation and adaptation research through a bibliometric review of history and evolution," *Energy Buildings*, vol. 287, May 2023, Art. no. 112976, doi: [10.1016/j.enbuild.2023.112976](https://doi.org/10.1016/j.enbuild.2023.112976).
- [75] B.-J. He, "Cause-related injustice, process-related injustice, effect-related injustice and regional heat action planning priorities: An empirical study in Yangtze river delta and Chengdu–Chongqing urban agglomerations," *Landscape Urban Plan.*, vol. 237, Sep. 2023, Art. no. 104800, doi: [10.1016/j.landurbplan.2023.104800](https://doi.org/10.1016/j.landurbplan.2023.104800).



Wenbo Yu is currently working toward the doctorate degree in land resources management with Northeastern University, Shenyang, China.

His current research interests include space time evolution of human settlements, urban thermal environment and urban landscape analysis.



Jun Yang received the Ph.D. degree in human geography from Liaoning Normal University, Dalian, Liaoning, China, in 2009.

He is a Professor in the effect of human settlement and GIS with Northeastern University. He has been committed to urban space growth, urban thermal environment, cellular automata land use change and urban human settlements and other aspects of research.



Nan Cong received the Ph.D. degree in physical geography from Beijing University, Beijing, China, in 2014.

She is currently with Institute of Geographic Sciences and Natural Resources Research, Chinese Academy of Sciences, Beijing, China. She conducts vegetation ecosystem and global change research based large-scale aerospace data.



Jiayi Ren is currently working toward the doctorate in land resources management with Northeastern University, Shenyang, China.

She has been committed to assessment of urban thermal environment and land use policy.



Huisheng Yu is currently working toward the doctorate in land resources management with Northeastern University, Shenyang, China.

He has been committed to assessment of ecosystem services, urban multicenter recognition, and other aspects of research.



Xiao Xiangming received the Ph.D. degree in ecology from Colorado State University, Fort Collins, CO, USA, in 1994.

He is a Professor with the School of Atmospheric and Geography, University of Oklahoma, Norman, Oklahoma, USA, and the Director of the Earth Observation and Modeling Office. He has been committed to land use and land cover change, carbon cycle, and ecological environment analysis of infectious diseases.



Jianhong Xia received the Ph.D. degree in geographic information science from Liaoning Normal University, Dalian, Liaoning, China, in 1996.

She has over 10 years' experience as a GIS Educator and Spatial Analyst and Modeler. She has also worked as a Transport Geographer and Transit Planner with a range of research experience in relation to tourism, public transport development, driving, spatial navigation and way finding and human mobility.